

# Modulation of proton-induced current fluctuations in the human nicotinic acetylcholine receptor channel

Christophe Danelon<sup>1</sup>, Jörg Grandl<sup>1</sup>, Ruud Hovius, Horst Vogel\*

Laboratory of Physical Chemistry of Polymers and Membranes, Ecole Polytechnique Fédérale de Lausanne, CH-1015 Lausanne, Switzerland

Received 20 April 2006; received in revised form 12 June 2006; accepted 13 July 2006

Available online 2 August 2006

## Abstract

The nicotinic acetylcholine receptor (nAChR) is a ligand-gated ion channel that switches upon activation from a closed state to a full conducting state. We found that the mutation  $\delta$  S268K, located at 12' position of the second transmembrane domain of the  $\delta$  subunit of the human nAChR generates a long-lived intermediate conducting state, from which openings to a wild-type like conductance level occur on a submillisecond time scale. Aiming to understand the interplay between structural changes near the 12' position and channel gating, we investigated the influence of various parameters: different ligands (acetylcholine, choline and epibatidine), ligand concentrations, transmembrane voltages and both fetal and adult nAChRs. Since sojourns in the high conductance state are not fully resolved in time, spectral noise analysis was used as a complement to dwell time analysis to determine the gating rate constants. Open channel current fluctuations are described by a two-state Markov model. The characteristic time of the process is markedly influenced by the ligand and the receptor type, whereas the frequency of openings to the high conductance state increases with membrane hyperpolarization. Conductance changes are discussed with regard to reversible transfer reaction of single protons at the lysine 12' side chain.

© 2006 Elsevier B.V. All rights reserved.

**Keywords:** Noise analysis; Current fluctuation; Ionizable site; Ion channel gating; Slow-channel syndrome

## 1. Introduction

The muscle-type nicotinic acetylcholine receptor (nAChR) is a ligand-gated ion channel responsible for synaptic transmission at the neuromuscular junction and is the archetypical example of the family of cys-loop receptors [1]. It was the first channel whose currents have been measured on a single-molecule level, which was a milestone in elucidating the molecular mechanisms of channel function [2]. High-resolution patch-clamp experiments have then shown that single-channel openings appear temporally clustered [3–5], suggesting a complex reaction scheme with multiple conformational states [6]. Additional complexity of nicotinic channel activity was highlighted by the observation of multiple and discrete subconductance states in

tissue-cultured embryonic rat muscle [7], embryonic chick muscle [8,9] and receptors purified and reconstituted from *Torpedo* membranes [10]. Multiple levels of conductance have been also observed in the other channels of the cys-loop family receptors, namely the  $\gamma$ -aminobutyric acid, glycine and serotonin receptors [11–13]. Sigworth reported that the nAChR from cultured rat muscle cells exhibits an excess variance of open-channel current [14]. Similar increase of current noise has been observed in nAChR of chick muscle [9] and rat muscle [7]. These current fluctuations were explained to stem from structural fluctuations in the pore [14,15]. More general, investigation of subconductance states has shown its usefulness to elucidate gating mechanisms in other channel proteins [16,17].

Reversible protonation of ionizable sites was shown to produce conductance fluctuations in various ion channels such as  $\text{Ca}^{2+}$  [18],  $\alpha$ -hemolysine [19], VDAC [20], OmpF [21] and mouse nAChR [22] channels. In the last example, Cymes et al. engineered protonable side chains along the channel lining

\* Corresponding author. Tel.: +41 21 693 3155; fax: +41 21 693 6190.

E-mail address: [horst.vogel@epfl.ch](mailto:horst.vogel@epfl.ch) (H. Vogel).

<sup>1</sup> The two authors contributed equally to this work.

second transmembrane segment (TM2) to probe local dielectric constants at the single amino acid level. Individual protonation–deprotonation events appeared as pH-dependent current fluctuations. Subconductance states assigned to ionic current restriction across the protonated pore have been observed. The orientation of side chains lining the helix relative to the ion pathway could be pointed out demonstrating the potential of the approach to elucidate structural aspects of the open pore.

The importance of TM2 in the gating process of the nAChR channel has been revealed by site-directed mutagenesis [22–32], site-directed labeling [27,33,34] and by structural electron microscopy studies [35,36]. The residue at position 12' of TM2 segment of the  $\delta$  subunit is well conserved among sequences of nAChR  $\delta$  subunits of vertebrate species and is closely related to the congenital myasthenic syndrome [37,38]. Therefore, mutations at this position have been studied intensively [22,29–31]. Further, this residue has a distinct contribution to nAChR activation with regard to the homologous position in the other subunits and its implication in both transmitter binding and channel gating has been shown [26].

Here, we show that the  $\delta$  S12'K mutation in TM2 of the human muscle nAChR exhibits similar activity than the homologous mouse receptor mutant [22], i.e. a stable subconductance state and rapid fluctuations to a high conductance level. Since the open channel transitions were not fully resolved in time, we used spectral noise analysis as a complement to dwell time analysis to determine the characteristic time constants of the fluctuations. Whereas structural and functional properties of  $\delta$  TM2 residues have been described in detail at constant conditions [22], we investigated the influence of the type of receptor (fetal or adult nAChR) and of different agonists, the ligand concentration and the transmembrane potential on the different gating kinetics.

We considered two mechanistic origins of the open channel current fluctuations: one model assumes that conductance changes are directly produced by proton exchange at the lysine 12' side chain, whereas the second model involves protein conformational changes. The results and their relevance for the channel gating pathway are discussed with regard to the structure of the closely related *Torpedo californica* acetylcholine receptor.

## 2. Materials and methods

### 2.1. Site-directed mutagenesis

cDNAs coding for the  $\alpha$ ,  $\beta$ ,  $\gamma$ ,  $\epsilon$  or  $\delta$  subunits (SWISSPROT; Acc: P02708, P11230, P07510, Q04844 and Q07001, respectively) of the human muscle nAChR in pcDNA 3 or pcDNA 3.1 expression vectors (Invitrogen, Basel, Switzerland) were used. Using the restriction sites of *Bam*HI and *Xba*I cDNA of the  $\delta$  subunit was subcloned into the cloning vector pBluescript II KS+ (Stratagene, La Jolla, CA) and the mutation S268K was produced with the QuikChange Site-Directed Mutagenesis Kit (Stratagene) protocol. After mutagenesis the construct was subcloned back into the original expression vector using the same restriction sites. The correctness of all cDNAs was confirmed by sequencing (MWG, Ebersberg, Germany). The identified background mutation  $\beta$  P15A located in the signal sequence did not show significant changes in  $EC_{50}$  and single-channel conductance compared to the wild-type receptors [39].

### 2.2. Cell preparation

Human embryonic kidney cells (HEK293) were cultured in D-MEM:F-12 medium (Invitrogen) with 2.5% fetal calf serum added, at 37 °C and in a humidified 5% CO<sub>2</sub> atmosphere. Cells were transiently transfected using the Effectene Transfectent Reagent (Qiagen, Hilden, Germany). A total of 0.2  $\mu$ g cDNA coding for the  $\alpha$ ,  $\beta$ ,  $\delta$  and  $\epsilon$  or  $\gamma$  subunits of the human muscle nAChR was mixed with green fluorescent protein (GFP) cDNA in the ratio of 2:1:1:1:1 ( $\alpha$ : $\beta$ : $\epsilon$  or  $\gamma$ : $\delta$ :GFP) and applied to a 35 mm culture dish with 2 ml medium. Experiments were carried out 1–3 days after transfection keeping cells in buffer containing NaCl 147 mM, glucose 12 mM, HEPES 10 mM, KCl 2 mM, MgCl<sub>2</sub> 1 mM, pH adjusted to 7.4 with NaOH (all Sigma, Buchs, Switzerland).

### 2.3. Patch-clamp recordings

Recordings were performed at 18 °C in buffer (see above) on cells that showed green fluorescence. Borosilicate patch pipettes (GB 150F-8P and GB 150TF-8P, Science Products, Basel, Switzerland) were pulled with a P-87 micropipette puller (Sutter Instruments, Novato, CA) and had a resistance of 5–10 M $\Omega$  when filled with a solution containing NaCl 140 mM, EGTA 10 mM (Sigma) and HEPES 10 mM pH adjusted to 7.4 with NaOH. Currents were measured with an EPC9 patch-clamp amplifier (HEKA, Lambrecht, Germany).

Whole-cell measurements were carried out at a holding potential of  $-60$  mV. Cells were continuously washed with buffer solution and the ligands acetylcholine (ACh), choline (Ch), epibatidine (Epi) (all Sigma, Buchs, Switzerland) at different concentrations were applied with a solution changer (RSC200, Bio-Logic, Claix, France) until the maximal response was reached. Data were sampled at 400 Hz and recorded using the program Pulse (HEKA). Peak currents were baseline corrected, normalized and fitted using IGOR Pro (WaveMetrics, Portland, OR) with the Hill equation:  $I = I_{\max} / (1 + (EC_{50}/[L])^n)$ , where  $I_{\max}$  is the maximal current upon application of 100  $\mu$ M ACh,  $[L]$  the agonist concentration,  $EC_{50}$  the agonist concentration at half maximal response and  $n$  is the Hill coefficient.

Single channel-measurements were carried out in the cell-attached configuration unless otherwise stated and the ligands were added to the pipette solution. The data were filtered with a Bessel filter at 2.9–8 kHz and sampled at 10–50 kHz. We studied the influence of ligand concentration by activating the fetal nAChR with 0.1  $\mu$ M, 1  $\mu$ M or 10  $\mu$ M of ACh. Effects of receptor and agonist types were investigated by activating the adult nAChR mutant with 10  $\mu$ M ACh, 50 nM Epi or 500  $\mu$ M Ch (Fig. 2A).

For each individual experiment, the applied voltage was corrected to account for the intrinsic cell membrane potential. Indeed, the averaged value is  $-32$  mV, but large range deviations from  $-5$  mV to  $-65$  mV have been observed, which justifies systematic voltage correction. Hence, all given voltages are true values with standard deviations of  $\pm 2$  mV. The hyperpolarizing voltage limit of a recording was determined by the electrical stability of the membrane and was typically  $-150$  mV. The low-magnitude voltage limit, which corresponds to a signal-to-noise ratio of about 1.6, was typically  $-20$  mV at 2.9 kHz bandwidth. We performed recordings at high positive applied voltages (reversed polarity), but the membrane seal became unstable.

### 2.4. Dwell time analysis

For each condition, segments of at least three different patches showing single-channel activity were selected and idealized using the SKM algorithm of QuB [40]. Histograms of dwell time distributions were fitted with exponential curves using Igor Pro and their means were calculated. Rate constants were obtained from a fit with a linear three-state model (MIL-algorithm) for each patch experiment, voltage, ligand concentration and ligand separately, by imposing a dead time of 90–100  $\mu$ s and by using a correction for missed events. The latter value was determined for each experimental condition by maximizing the likelihood of fits to dwell time distributions. Two components were observed in the shut time histograms. The slower component (mean value  $\sim 1$  ms) refers to shut events within a burst while the longer time component (hundreds ms) refers to time lags between bursts. Then, bursts were defined as a series of closely spaced openings into a conducting state that was longer than 20 ms and

preceded and followed by closed intervals greater than a specified critical time  $t_{crit}$ . The value of  $t_{crit}$  was obtained by the upper limit of the slower component and was usually about 5 ms (similar values were obtained by taking 4-fold longer time than the mean). Therefore, shut states with dwell times shorter than  $t_{crit}$  belong to a burst (see upward transitions indicated by arrows in Fig. 1A), while longer shuts separate bursts from each other.

### 2.5. Power spectral analysis

Trace segments (512 points at 100  $\mu$ s / point) in the background and open channel levels were selected for power spectra calculation using the following exclusion criteria [14]: (i) Too short channel openings; (ii) openings having closing spikes; (iii) overlapping openings due to simultaneous activation of

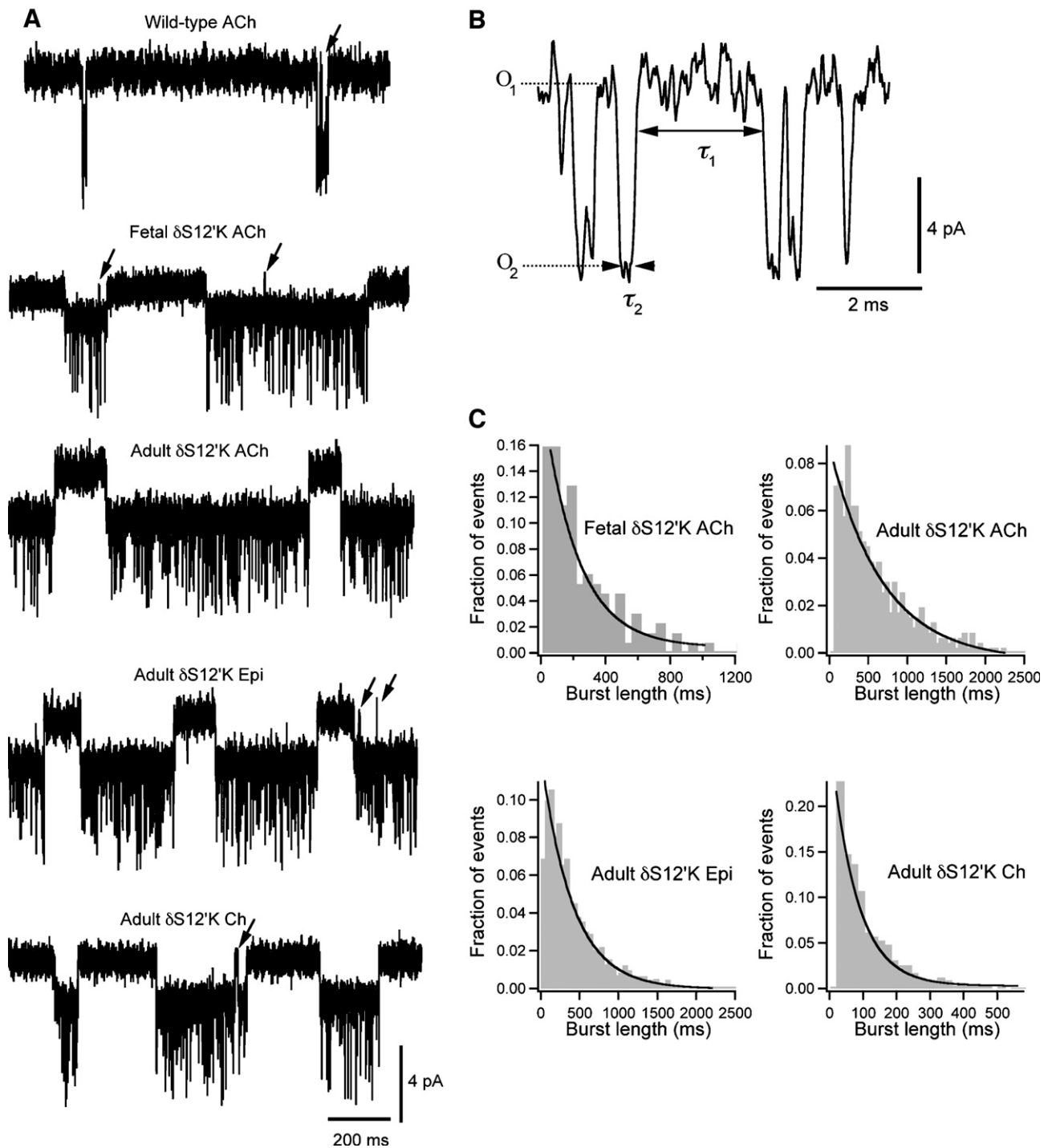


Fig. 1. Effect of  $\delta$  S268K mutation in the human nAChR. (A) Single-channel current traces of  $\gamma$ - and  $\epsilon$ -nAChR mutants, stimulated by 10  $\mu$ M ACh, 50 nM Epi and 500 mM Ch at pH 7.4 and 2.9 kHz bandwidth. Downward deflections are channel openings. Brief closures within bursts are indicated by arrows. A current trace of the wild-type  $\epsilon$ -nAChR activated by 10  $\mu$ M ACh is shown for comparison. (B) An enlargement of the current trace of the fetal-type receptor mutant activated by ACh shows that some transitions from the first conductance state  $O_1$  to the second state  $O_2$  get resolved at 5 kHz filtering. The levels of channel current  $i_1$  and  $i_2$  as well as respective lifetimes  $\tau_1$  and  $\tau_2$  are indicated. (C) Burst-length histograms of  $\gamma$ - and  $\epsilon$ -nAChR mutants fitted with exponential curves. The fitted values are given in Table 1.

several channels. In the cell-attached configuration, the variations of the background standard deviation expressed in percent of the mean value are  $\sim 20\%$  between patches and  $\sim 6\%$  between segments of the same patch (Fig. 2C). To account for this experimental variability, two procedures have been followed. First, the true spectrum of the channel current fluctuations reflecting the open channel noise excess was obtained by subtracting the averaged background spectrum from the averaged open channel spectrum. Second, background spectra were accumulated from shut state segments adjacent to open channel events in order to reduce the spectral contribution from any changes in the fluctuations of the baseline [14].

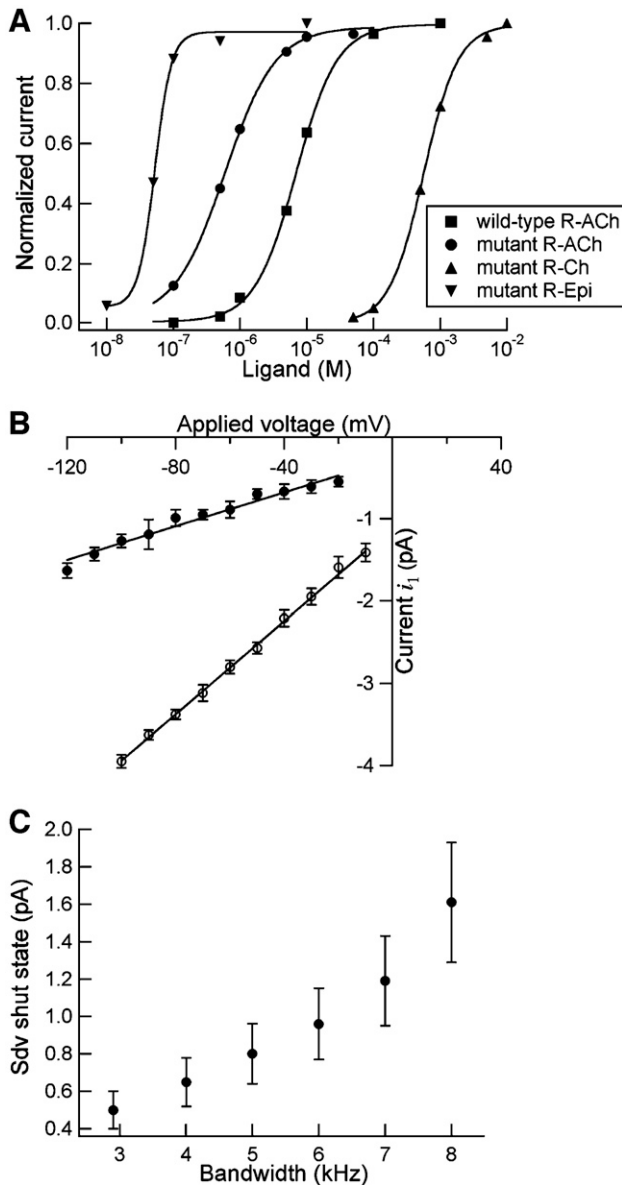


Fig. 2. Dose–response curves, voltage calibration and background current noise. (A) Concentration–response curves of wild-type and  $\gamma$ -nAChR mutant, activated by ACh, Ch and Epi. The Hill equation was used to fit the experimental data. Values of  $EC_{50}$  are  $6.9 \pm 0.3 \mu\text{M}$  (■),  $594 \pm 55 \text{ nM}$  (●),  $565 \pm 23 \mu\text{M}$  (▲) and  $53 \pm 3 \text{ nM}$  (▼). (B) Single-channel current amplitude  $i_1$  as a function of the externally applied potential for the fetal (●) and the adult (○) mutants. The single-channel conductance  $g_1$  can be determined from the slope of a linear fit and the intrinsic membrane potential by its interpolation and intersection at zero current. Two individual on-cell experiments having resting cell potentials of about  $-20 \text{ mV}$  and  $-40 \text{ mV}$  are shown. (C) Standard deviation of the current baseline as a function of the bandwidth.

### 3. Results

#### 3.1. Functional effect of the $\delta$ S12'K mutation on the human nAChR

A single point mutation that changes serine into lysine at position 12' of the TM2 segment of the  $\delta$  subunit ( $\delta$  S268K) generates an unusual channel behavior upon agonist activation in patch-clamp experiments (Fig. 1A). Two features are clearly seen. First, channel openings appear as long-lived events compared to the wild-type receptor (Fig. 1A, C). Short closing events within bursts similarly to wild-type activity are observed (Fig. 1A, arrows). Second, opening events consist of a subconductance level interrupted by brief sojourns towards larger conductance. The persistence of this behavior is demonstrated on both fetal-type and adult-type receptors ( $\gamma$ -nAChR and  $\epsilon$ -nAChR, respectively, the  $\gamma$  subunit being replaced by the  $\epsilon$  subunit during maturation) activated by ACh, Ch or Epi.

The following control experiments were performed: (i) cells were transfected with cDNA encoding the nAChR subunits omitting the mutated  $\delta$  subunit. No activity could be identified upon ACh addition. This demonstrates that the channel activity observed (Fig. 1A) is indeed due to nAChRs comprising  $\delta$  S12'K and thus that the mutation does not compromise incorporation of the  $\delta$  subunit during receptor assembly; (ii) no channel opening is observed in cells expressing  $\delta$  S12'K containing nAChR in absence of agonist, demonstrating that ligand binding triggers the reported process.

The lifetime of large conductance channel openings is too short to be fully time resolved at 2.9 kHz bandwidth (Fig. 1A) leading to a heterogeneous distribution of amplitudes. Recordings carried out at 5 kHz bandwidth show that most of the current transitions of the  $\gamma$ -nAChR channel mutant reach a well-defined high current level (Fig. 1B). The diliganded receptor switches from the closed state C to the subconductance state  $O_1$  or the full conductance state  $O_2$ . Mean open-channel currents are correspondingly  $i_1$  and  $i_2$ . Fig. 2B shows a plot of  $i_1$  versus the applied voltage for the  $\gamma$ -nAChR (upper curve) and the  $\epsilon$ -nAChR (lower curve), measured at 2.9 kHz filter frequency. The respective conductance values  $g_1$  are  $12 \pm 2 \text{ pS}$  and  $25 \pm 2 \text{ pS}$ , with no apparent dependency on the type of agonist. Occasionally, bursts with both  $i_1$  and  $i_2$  having  $\sim 40\%$  lower values are observed within the same trace. Moreover, direct transitions from the shut state to the fully open state, as well as low-conductance transitions without fast flickerings occasionally occur. Latter events were also observed when studying the wild-type receptor [41]. In the following, we did not analyze rare channel activities deviating from those shown in Fig. 1A.

#### 3.2. Kinetic analysis of the open-closed gating

First, we investigated the slow-kinetics component of channel activity, i.e. the open-closed gating. The values of the averaged burst lifetime (or mean open channel duration)  $\tau_b$ , mean times of the shut (C) and open states ( $O_1 + O_2$ ) within

a burst  $\tau_s$  and  $\tau_o$ , respectively, and the resulting apparent gating constant  $\Theta = \tau_o/\tau_s$  obtained for different ligands and subunit compositions are displayed in Table 1. Within the accuracy of the measurements we did not identify an influence of the membrane potential on these lifetimes. Therefore, the reported data are averaged over the studied voltages. The results show a pronounced variation of time constants with both the different agonists and receptor subunit composition. As an example, the burst lifetimes of  $\varepsilon$ -nAChRs are  $757 \pm 159$  ms and  $77 \pm 4$  ms when activated by ACh and Ch, respectively (Fig. 1C, Table 1).

### 3.3. The open channel noise is described by a two-state Markov model

Time-dependent current fluctuations in the shut state (background) and open channel state were analyzed in the frequency domain using power spectral densities. Fig. 3A shows typical averaged spectra of open channel segments and adjacent background segments for the ACh-activated  $\gamma$ -nAChR at  $-130$  mV. The amplitude of the spectral density caused by the opening of a channel is particularly large at low frequencies. Above 3 kHz the background noise is dominating, limiting the spectral analysis to the frequency range 20 Hz–2.5 kHz.

Fig. 3B, C show that open channel noise spectra computed for all combinations of receptor types, ligands and voltages can be fitted over the frequency range of two decades by a Lorentzian function:

$$S(f) = \frac{S_0}{1 + (f/f_c)^2}, \quad (1)$$

where  $S_0$  is the low-frequency limit of the spectrum amplitude and  $f_c$  is the corner frequency. Such spectra are characteristic of a two-state Markov reaction where the channel switches between two conductance levels (as observed at 5 kHz bandwidth recordings in Fig. 1B) with current fluctuations following a first-

order relaxation process. The relaxation time constant  $\tau$  of the reaction is related to the corner frequency and the mean lifetimes  $\tau_1$  and  $\tau_2$  in states  $O_1$  and  $O_2$  by:

$$\tau = \frac{1}{2\pi f_c} = \frac{\tau_1 \tau_2}{\tau_1 + \tau_2}, \quad (2)$$

The low-frequency limit of the spectrum is defined as [42]:

$$S_0 = \frac{4(\Delta i)^2 \tau^2}{\tau_1 + \tau_2}, \quad (3)$$

where  $\Delta i$  is the difference in current level of states  $O_1$  and  $O_2$ . Although transitions to the high conductance state are not time-resolved at 2.9 kHz bandwidth, the corresponding spectral density contains all accessible parameters governing current fluctuations.

### 3.4. Conditions affecting the open channel noise

The membrane potential does not affect the corner frequency for ACh-induced openings of the  $\gamma$ -nAChR, whereas the noise amplitude increases with membrane hyperpolarization (Fig. 3B). Inversely, activation of  $\varepsilon$ -nAChR by the different agonists affects the corner frequency, but has little influence on the low-frequency amplitude (Fig. 3C). Channel activation by Epi and Ch leads to a significant shift of the Lorentzians towards higher frequencies as compared to ACh-induced open channel noise. Comparison of noise spectra obtained for  $\gamma$ - and  $\varepsilon$ -nAChRs activated by ACh shows that the relaxation process of current fluctuations, as characterized by the corner frequency, is slower for the  $\varepsilon$ -nAChR. Open channel conductance changes are equilibrated, since the characteristic time constants of the gating do not depend on the burst lifetime, the length of current recordings or the position of the open channel segments within a burst.

The relaxation times  $\tau$  derived from Eq. (2) and the low-frequency amplitudes, pooled from 18 patches by stimulation with different agonists or several ACh concentrations, are plotted in Fig. 4 as a function of voltage. The large data scattering mainly arises from variability between patches, as will be discussed later, and was particularly pronounced for the  $\varepsilon$ -nAChR mutant channel activated by 10  $\mu$ M ACh. Fig. 4A, B show that there is no substantial influence of ACh concentration and voltage (see also Fig. 3B) on the relaxation time constant. Averaged values of  $\tau$  over the voltage range are:  $152 \pm 29$   $\mu$ s for ACh-activated  $\gamma$ -nAChR ( $n=8$ );  $200 \pm 41$   $\mu$ s for ACh-activated  $\varepsilon$ -nAChR ( $n=4$ );  $125 \pm 14$   $\mu$ s for Epi-activated  $\varepsilon$ -nAChR ( $n=3$ );  $112 \pm 12$   $\mu$ s for Ch-activated  $\varepsilon$ -nAChR ( $n=3$ ). Relaxation times decrease along the series  $\varepsilon$ -nAChR (ACh) >  $\gamma$ -nAChR (ACh) >  $\varepsilon$ -nAChR (Epi)  $\sim$   $\varepsilon$ -nAChR (Ch). This result demonstrates that the correlation time of current fluctuations is affected by the type of ligand and the composition of receptor subunits, but not significantly changed by ACh concentration and transmembrane voltage.

No consistent differences were observed for values of  $S_0$  with ACh concentration (Fig. 4C). The apparent tendency of  $S_0$

Table 1  
Averaged time constants for the slow-kinetic reaction

Receptor	Ligand	Burst lifetime $\tau_b$ (ms)	Open time $\tau_o$ (ms)	Shut time $\tau_s$ (ms)	Apparent gating constant $\Theta$
wild-type	ACh	2.13	0.55	0.02	28
$\gamma$ -nAChR	ACh	$215 \pm 36$	$74 \pm 10$	$0.4 \pm 0.1$	$185 \pm 71$
$\varepsilon$ -nAChR	ACh	$757 \pm 159$	$205 \pm 27$	$1.1 \pm 0.2$	$189 \pm 68$
	Epi	$408 \pm 20$	$109 \pm 9$	$1.7 \pm 0.3$	$65 \pm 16$
	Ch	$77 \pm 4$	$62 \pm 6$	$0.5 \pm 0.1$	$133 \pm 27$

Burst lifetimes  $\tau_b$ , mean open times  $\tau_o$ , mean shut times  $\tau_s$  and apparent gating constants  $\Theta$  for the transition between the closed state and the conducting state  $O_1$  or  $O_2$ , inferred from dwell time analysis and histogram fits. Receptors were activated with 10  $\mu$ M ACh, 50 nM Epi or 500  $\mu$ M Ch. Both  $\gamma$ -nAChR and  $\varepsilon$ -nAChR were  $\delta$  S268K mutants. Values for the wild-type refer to human  $\varepsilon$ -nAChRs expressed in HEK cells and are taken from Sine and coworkers [74]. Similar values have been reported by another group [75]. When expressed in *Xenopus* oocytes, the mean burst lifetimes are  $\sim 8$  ms and  $\sim 4$  ms for the human  $\gamma$ - and  $\varepsilon$ -nAChR channels, respectively [39].

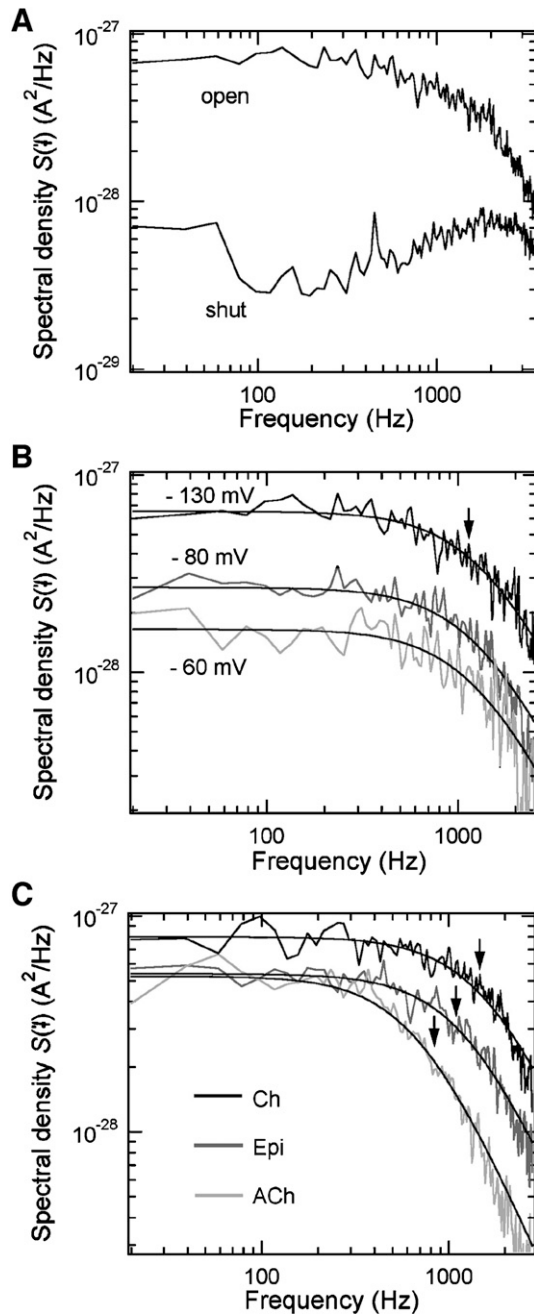


Fig. 3. Noise analysis of open-channel current. (A) Averaged power spectral densities of shut-state segments and open-state segments for the  $\gamma$ -nAChR activated by ACh. At high frequencies the magnitude of the background noise decreases due to low-pass filtering. (B) Power spectra of ACh-induced open-channel noise of the  $\gamma$ -nAChR obtained after background noise subtraction and recorded at different voltages. Voltage values correspond to applied potentials corrected for the resting membrane potential. Corner frequencies and plateau values of the Lorentzians, as determined from Eq. (1), are: 1252 Hz and  $1.7 \times 10^{-28} \text{ A}^2/\text{Hz}$  for -60 mV; 1285 Hz and  $2.7 \times 10^{-28} \text{ A}^2/\text{Hz}$  for -80 mV; 1350 Hz and  $6.5 \times 10^{-28} \text{ A}^2/\text{Hz}$  for -130 mV. (C) Power spectra for  $\epsilon$ -nAChR mutant stimulated with ACh, Epi and Ch at  $-110 \pm 2$  mV corrected voltage. Corner frequencies and plateau values of the Lorentzians are: 685 Hz and  $5.3 \times 10^{-28} \text{ A}^2/\text{Hz}$  for ACh; 1242 Hz and  $5.4 \times 10^{-28} \text{ A}^2/\text{Hz}$  for Epi; 1606 Hz and  $4.5 \times 10^{-28} \text{ A}^2/\text{Hz}$  for Ch (the amplitude of this spectrum has been multiplied by 1.8 for visibility). Corner frequencies are indicated by arrows. The errors of the Lorentzian fits are less than 15% for  $f_c$  and less than 10% for  $S_0$ .

to be larger for activation of  $\epsilon$ -nAChR by ACh seems to be due to patch-to-patch variations (Fig. 4D). The increase with membrane hyperpolarization is more pronounced. Such an effect can be expected from Eq. (3), but we investigated the magnitude of this voltage dependence in more detail. Assuming that the relationship between  $\Delta i$  and the voltage is ohmic (this is verified in Fig. 7), a quadratic dependency of the power spectral density on the voltage is expected if the frequency of openings to the high conductance state, defined as  $\nu = (\tau_1 + \tau_2)^{-1}$ , is voltage independent [42,43]. For convenience, a logarithmic representation would give rise to a slope of two, according to:

$$\log S_0 = \log(4(\Delta g)^2 \tau^2 \nu) + 2 \log V, \quad (4)$$

where  $V$  is the corrected voltage and  $\Delta g = \Delta i/V$ . Fig. 5A, B show a deviation of the fitted slope values (solid lines) of  $1.5 \pm 0.2$  and  $1.2 \pm 0.2$ , respectively for  $\gamma$ - and  $\epsilon$ -nAChR channels, with respect to a slope of two (dashed lines). Calculating the slope for each ligand condition, values  $< 2$  were systematically obtained. A second way to analyze the voltage dependency of the spectral density is depicted in Fig. 5C, D. The absolute variance of current fluctuations, calculated as  $\sigma^2 = S_0/4\tau$ , is plotted as a function of the open channel current  $i_1$  [14]. The same deviation is observed with slopes of  $1.6 \pm 0.1$  and  $1.2 \pm 0.2$  for the  $\gamma$ - and  $\epsilon$ -nAChRs, respectively. Taken together, these results indicate that the current noise arises from voltage-dependent conductance fluctuations.

### 3.5. Combining noise analysis and dwell time analysis

In the classical dwell time analysis a single channel recording is idealized by a trace containing well-defined conductance levels with ideally sharp transitions. Evaluation of open-time and closed-time distributions leads to the rate constants of the reaction. This requires that the conductance levels have discrete known values and that the events can be resolved in time. If the characteristic time of current fluctuations is not too short compared to the time resolution, missed events can be estimated and the histograms of dwell times calculated [40,44].

However, for the current fluctuations between the open states  $O_1$  and  $O_2$  obtained from traces acquired at 2.9 kHz bandwidth, as described before, idealization does not provide a good estimate of  $\Delta i$ , since high conductance events are not resolved. Values of the individual time constants  $\tau_1$  and  $\tau_2$  are significantly affected by the choice of the dead-time, but variations of their ratio are low ( $< 3\%$  deviation in  $\tau_1/\tau_2$  for a change of dead-time of 10  $\mu\text{s}$ ). Therefore, the apparent equilibrium constant, defined as  $K = \tau_1/\tau_2$ , can be determined with a good confidence level. Fig. 6A shows the apparent equilibrium constant as a function of the voltage for different ligands and receptor types. The effect of the voltage is similar for all conditions of receptor activation with values of  $K$  about 2-fold larger at -20 mV than at -160 mV.

The probability  $p$  to be in the state  $O_2$  can be calculated from the apparent equilibrium constant, according to  $p = (1 + K)^{-1}$ .

The mean lifetimes in states  $O_1$  and  $O_2$  are respectively given by:

$$\tau_1 = \frac{\tau}{p}, \text{ and } \tau_2 = \frac{\tau}{1-p}. \quad (5)$$

According to Eq. (5), we obtain values of  $\tau_2$  deviating by less than 10% from  $\tau$ , whereas  $\tau_1$  is at least 10-fold larger than  $\tau$ . The frequency of large openings can be expressed as:

$$\nu = \frac{p(1-p)}{\tau}. \quad (6)$$

Fig. 6B demonstrates that  $\nu$  rises with membrane hyperpolarization. The frequency is about 4 times larger at  $-150$  mV than at  $-40$  mV.

The last parameter to be determined in order to have a complete description of current fluctuations is the change of current between the subconductance state and the large conductance level. At high voltages and 5 kHz bandwidth two distinct current populations corresponding to  $i_1$  and  $i_2$  are

visible in the amplitude histogram and the occupancy of each state can be extracted (Fig. 6A, inset). However, this approach cannot be generalized to all conditions of voltages and ligands. Estimating  $\Delta i$  and  $p$  directly from the mean value  $\langle I \rangle$  and the absolute variance  $\sigma^2$  of current fluctuations was attempted using the equations:  $\langle I \rangle = \Delta i p$  and  $\sigma^2 = (\Delta i)^2 p(1-p)$ . Here again, this evaluation fails, since many missing short events of low amplitudes lead to underestimated values of  $p$ , especially at low voltages. According to Eq. (3) and Eq. (6), the current change  $\Delta i$  can be written as:

$$\Delta i = \left( \frac{S_0}{4\tau} \cdot \frac{1}{p(1-p)} \right)^{1/2}, \quad (7)$$

where  $p$  is calculated from dwell time analysis. Values of the full open channel current  $i_2 = i_1 + \Delta i$  are plotted as a function of the voltage for  $\gamma$ - and  $\epsilon$ -nAChRs (Fig. 7). The slopes of current–voltage characteristics for both intermediate and full open channels are constant in the voltage range studied and do not depend on type or concentration of agonist. Channel conductances  $g_1$

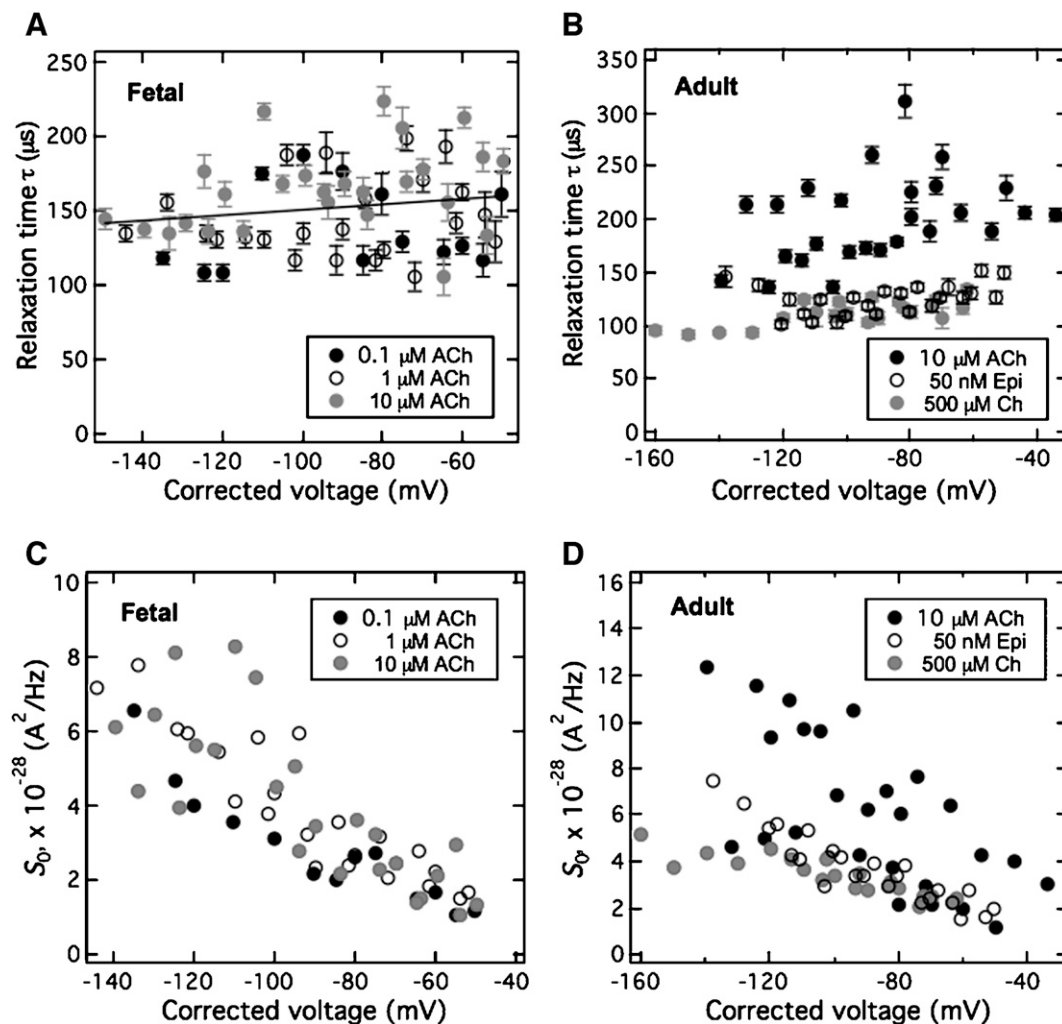


Fig. 4. Voltage-dependence of Lorentzian parameters. Relaxation times  $\tau$  (A and B) and low-frequency amplitudes  $S_0$  (C and D), obtained from Lorentzian fits to power spectral densities, as a function of the corrected voltage for fetal and adult nAChR channel mutants. The errors are less than 15% for  $\tau$  and less than 10% for  $S_0$  (error bars not displayed in Fig. 4C, D).

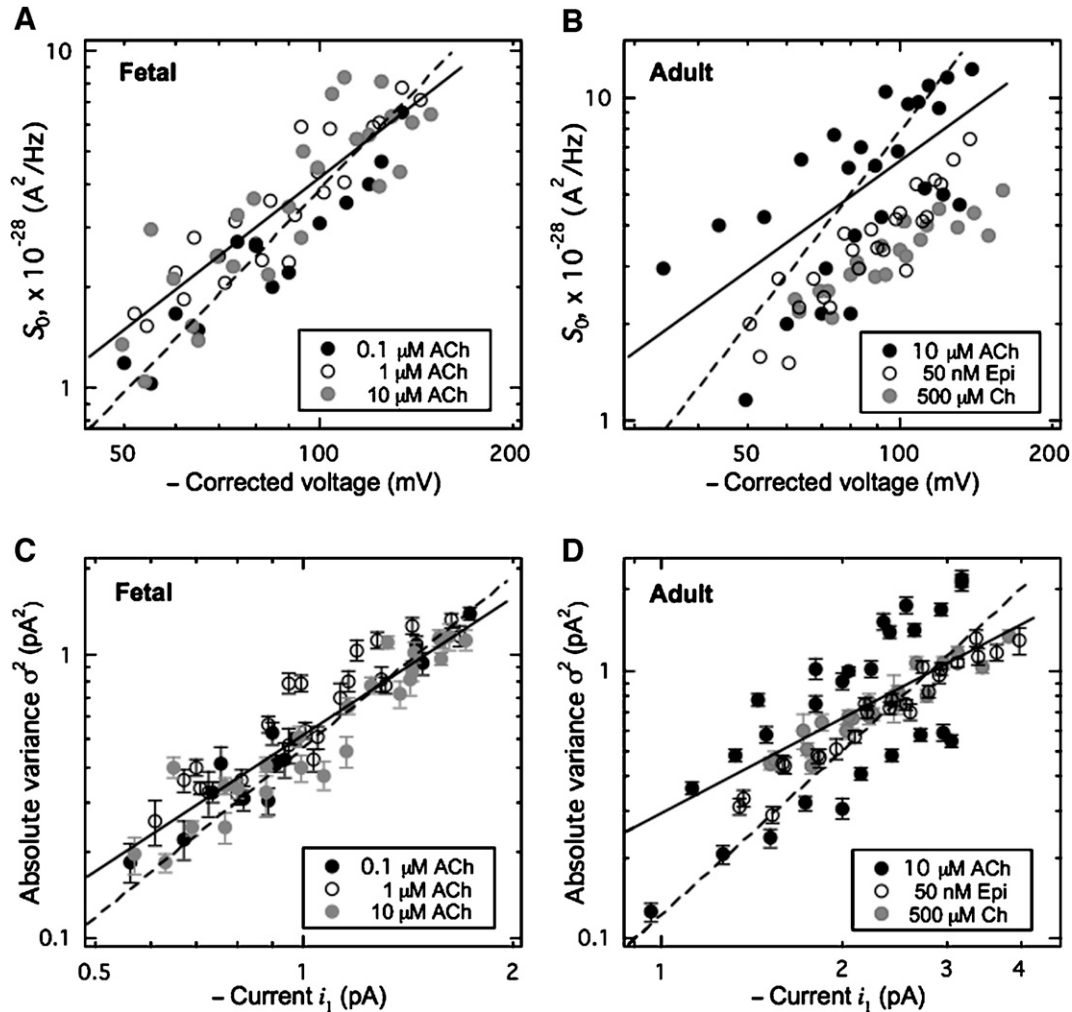


Fig. 5. (A and B) Logarithmic plots of low-frequency amplitudes  $S_0$  as a function of the absolute value of the corrected voltage. (C and D) Absolute variance  $\sigma^2$  of current fluctuations calculated from  $S_0$  and  $\tau$  (Fig. 4) and plotted as a function of  $-i_1$ . Solid lines are fits to the data and dashed lines are fits with an imposed slope of 2, as would be expected if current noise is produced by voltage-independent conductance fluctuations. For all fits, slopes  $<2$  are obtained.

and  $g_2$  are  $12 \pm 2$  pS and  $40 \pm 3$  pS for the  $\gamma$ -nAChR and  $25 \pm 2$  pS and  $57 \pm 4$  pS for the  $\epsilon$ -nAChR. It has to be noted that the conductance  $g_2$  is identical to that of the wild-type channel for both  $\gamma$ - and  $\epsilon$ -nAChRs [39]. Interestingly, the  $\gamma$  and  $\epsilon$  subunits affect differently the extent of channel blocking, defined as  $(g_2 - g_1)/g_2$ , of which values are  $0.70 \pm 0.17$  for the  $\gamma$ -nAChR and  $0.56 \pm 0.14$  for the  $\epsilon$ -nAChR.

#### 4. Discussion

##### 4.1. Possible mechanistic origins of proton-induced current fluctuations

The introduction of a lysine residue at the 12' position of the  $\delta$  subunit increases burst lifetimes and generates transient partial channel blocking events (Fig. 1A). These two features are preserved for various agonists and for the  $\gamma$ - and  $\epsilon$ -nAChRs. The conductances of the full openings are identical to those of the corresponding wild-type receptors. The homologous mutation in  $\alpha$  or  $\gamma$  subunit leads to similar channel activity, whereas receptors containing the mutation in  $\beta$  or  $\epsilon$  subunit open either

to a large or an intermediate conducting state [45]. The different channel activities highlight the functional asymmetry of the transmembrane segments [45].

Multiple levels of conductance in nAChR have been proposed to arise from positive cooperativity between channels in a membrane patch [46,47]. Our data cannot be interpreted in terms of conductance superimposition from identical neighboring channels, because (i) both conductance and kinetics of the two states are distinct, (ii) the relative conductance values of the two states are different between the  $\gamma$ - and  $\epsilon$ -nAChRs (Fig. 7). The arrangement of the subunits in different channel subtypes [25,48,49] can also be ruled out, since independent low- and high-conductance openings are very rarely observed. Also, currents were not observed after omission of the  $\delta$  subunit. Moreover, the frequency of full channel openings does not depend on the agonist (ACh) concentration in the range of 0.1  $\mu$ M to 10  $\mu$ M. Channel blocking by the agonist can be excluded as a reason for fast gating transitions, since such effects occur at concentrations  $>300$   $\mu$ M for ACh [50,51]. Curare-stimulated nAChR also displays transitions from a subconductance state to a full conductance state, but it is the

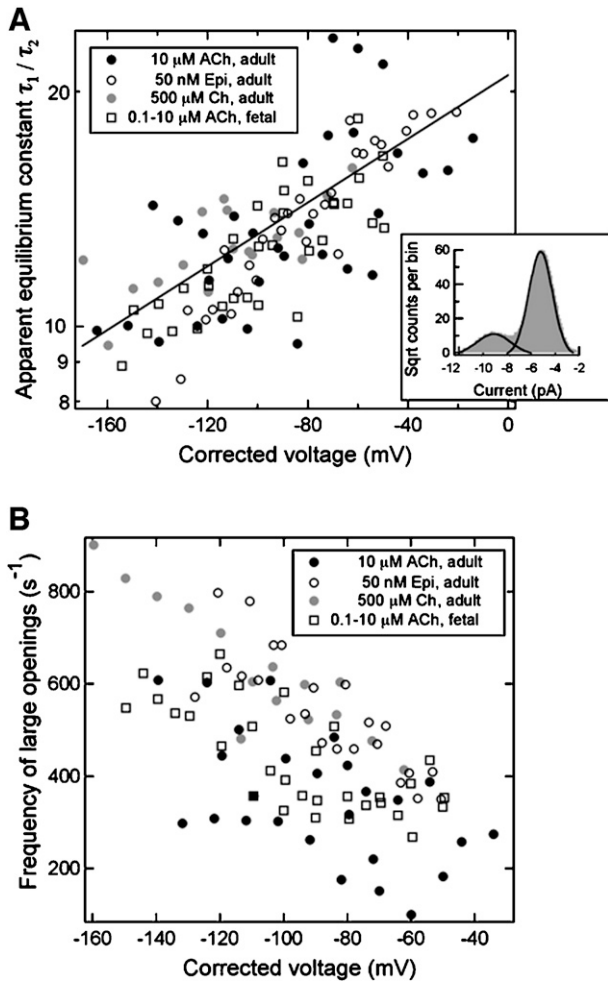


Fig. 6. (A) Semi-logarithmic representation of the apparent gating equilibrium constants  $K = \tau_1/\tau_2$ , inferred from dwell time analysis, as a function of the corrected voltage. Values of the change of the molar dipole moment of the system,  $\Delta M$ , occurring during  $O_1 \rightleftharpoons O_2$  transitions, are determined according to Eq. (9) for both fetal and adult nAChR channel mutants (straight line). The inset shows an amplitude histogram (square root of number of events per bin) of open state currents measured at 5 kHz bandwidth. At this filter frequency the state  $i_2$  is resolved so that current differences  $\Delta i$  and occupancies can be obtained from Gaussian fits. (B) Opening frequency into the conductance state  $O_2$  is calculated from Eq. (6) and plotted as a function of the corrected voltage.

partial channel block by curare that limits the flow of ions [52,53]. We conclude that the original gating process comprising two time-separated conductance levels arises from ligand activation of isolated single-channel mutants.

Similar channel characteristics to those reported here, namely long-lived bursts and partial channel block, were observed at pH 7.4 for the mouse  $\delta$  S12'K  $\epsilon$ -nAChR mutant [22]. Human and mouse nAChRs have a high sequence homology of their pore lining domains TM2 and TM3. Their TM2 domains only differ at the 5' position in the  $\gamma$  subunit (an isoleucine in human, a threonine in mouse) (Fig. 8A). In rat nAChR, this residue exchange was found to affect only the channel conductance [54]. The ionization states of natural lysines at position 9' and 29' (Fig. 8A) are fixed at pH 7.4 in the mouse receptor. Indeed, the lysine at 9' is oriented away from the channel lumen and it is completely deprotonated, whereas

the lysine at 29' is predominantly protonated [22]. Therefore, open channel current fluctuations occurring in the mouse and, by extension, in the human  $\delta$  S12'K receptor mutants would exclusively reflect protonation–deprotonation events of the lysine 12' side chain. Following the model used by Cymes et al. [22], the extra positive charge carried by the protonated lysine restricts cation permeation leading to the partially open pore. Thus, current transitions from  $O_1$  to  $O_2$  refer directly to single deprotonation events, while reverse transitions refer to single protonation events. The deprotonation rate constant ( $s^{-1}$ ) is  $\tau_1^{-1}$  and the protonation rate constant ( $M^{-1} s^{-1}$ ) is  $\tau_2^{-1} \times 10^{pH}$ . The model predicts that  $\tau_1$  should be pH independent. The  $pK_a$  of individual lysine side chains, which reflects the local environment of the protonable groups, can be evaluated by  $pK_a = \log K + pH$ . From our data, it follows that  $pK_a$  values are slightly voltage dependent ranging at pH 7.4 between  $\sim 8.4$  at  $-160$  mV and  $\sim 8.7$  at zero voltage. A  $pK_a$  of 8.9 ( $V \sim -100$  mV) was calculated for the lysine side chain at the homologous position in the mouse nAChR [22] suggesting that the 12' residue senses similar microenvironment in the open state of both receptors. Individual protonation–deprotonation rate constants are also in good agreement. Interestingly, the extent of channel blocking, which reflects lysine exposure to the channel lumen, is 0.56 for the  $\epsilon$ -nAChR (0.60 for the mouse receptor, see ref. 22) and 0.70 for the  $\gamma$ -nAChR indicating that the additional positive charge inside the channel (lysine protonated) affects the cationic current of the fetal receptor to a larger extent than the adult receptor. Importantly, we found that the protonation rate constant of the lysine 12' is modulated by the ligand (Fig. 4B) demonstrating that the kinetics of proton exchange would not be decoupled from agonist-specific interactions and receptor type.

An alternative mechanism of proton-induced current fluctuations has been evidenced in L-type  $Ca^{2+}$  channels [55,56].

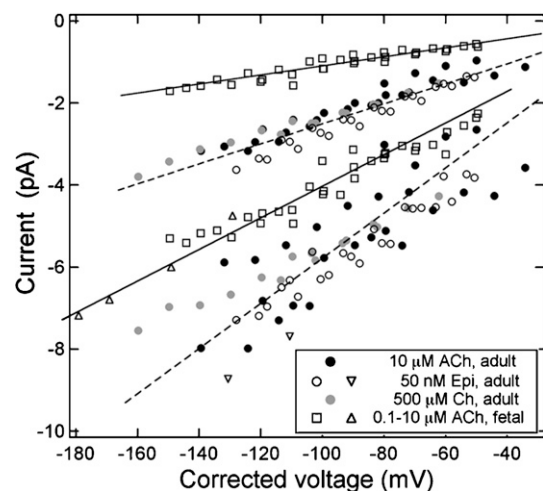


Fig. 7. Channel currents  $i_1$  (two upper curves) and  $i_2$  (two lower curves) as a function of the corrected voltage. Current  $i_2$  is defined as  $i_1 + \Delta i$  with  $\Delta i$  calculated according to Eq. (7). At  $V < -100$  mV, values of  $i_2$  can directly be derived from amplitude histograms (such as in Fig. 6A, inset) obtained at 5 kHz bandwidth recordings and were added as symbols  $\Delta$  and  $\nabla$  for the fetal- and adult-type receptor mutants, respectively. Linear fits of the data (forced through zero) for  $\gamma$ -nAChR (full line) and for  $\epsilon$ -nAChR (dashed line) demonstrate the ohmic behavior of both  $O_1$  and  $O_2$  states.

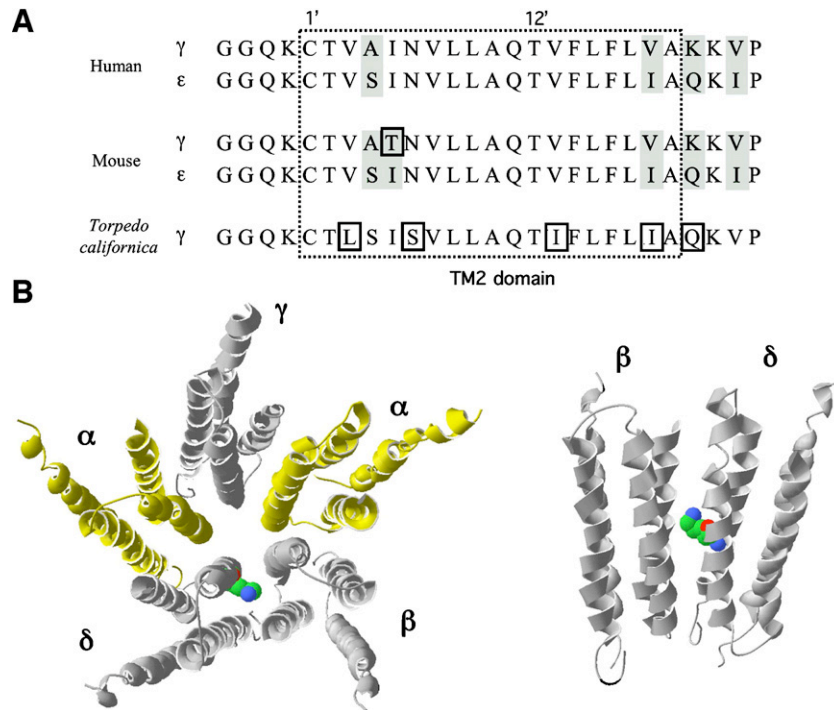


Fig. 8. (A) Sequence alignment of TM2 domains of human, mouse and *Torpedo californica*  $\gamma$  and  $\epsilon$  nAChR subunits. Residues highlighted in gray indicate differences between the two subunits of a given species. Boxed residues indicate differences compared to the sequence of human  $\gamma$ -nAChR. (B) Top view (left) and side view (right) of ribbon representation of the transmembrane helix bundles from the 4 Å resolution refined structure of *Torpedo californica* nAChR [36]. The native serine residue at position 12' in TM2 of the  $\delta$  subunit was replaced by a lysine without energy optimization. Carbon and nitrogen atoms of the lysine are green and blue spheres, respectively. The  $\alpha$  subunits are colored in yellow. (For interpretation of the references to colour in this figure legend, the reader is referred to the web version of this article.)

Contrary to the simple two-state model proposed above in which the high and low conductances represent the open-deprotonated and open-protonated channel states, respectively, the model described by Hess and his colleagues implies indirect allosteric, rather than direct electrostatic, interactions between the protonation site and the conducting ions. As a fundamental difference, the mean lifetimes in the high and low conductance levels no longer refer to the protonation kinetics since proton binding leads to reduced conductance by promoting a conformational change of the channel. However, the power spectrum of the open channel noise still has a single Lorentzian shape [55]. An interpretation would be that the protonated lysine side chain becomes destabilized in the high conductance state. In the general kinetic model, protons can also bind to the subconductance state with the consequence that the mean lifetime in the low conductance level becomes pH dependent. Our results show that the protein conformational changes that might cause conductance changes would be sensitive to the bound ligand.

No clear relationship between slow-kinetic (open-closed transitions) and fast-kinetic (open channel noise) parameters as a function of agonist is noticeable. As an example, the relaxation time constants with Ch and Epi are similar (Fig. 4B), but the burst lifetime is 5-fold larger with Epi than with Ch (Table 1). This further suggests that the two gating processes, even if they both originate from the lysine substitution, have distinct and non-cooperative molecular mechanisms. Fig. 2A shows that the  $\delta$  S12'/K mutation induces a shift of the dose–response curve

toward lower concentrations of ACh. The influence of the agonist on the mean lifetime in state  $O_2$  (Fig. 4B) indicates that the residue at the  $\delta$  12' position is not only involved in the gating of the nAChR pore, but also (indirectly) in the binding of the transmitter [26].

The spectral analysis of ionic current through membrane channels requires no initial gating model and is suited to investigate systems where single-channel gating events are not resolved [57]. This approach has been followed to study synaptic activity under application of agonists-inhibitors in multi-channel experiments [58–61] and to analyze single-channel recordings with transitions of brief lifetime or low amplitude [14,62]. As shown in Fig. 3, power spectra of open-channel current fluctuations can be fitted by a single Lorentzian in the range of 20 Hz–2.5 kHz for ACh, Ch and Epi application. The relaxation time constant and the variance of current fluctuations are extracted for each condition of agonist concentration, receptor type and transmembrane voltage. The scattering of  $S_0$  and  $\tau$  (Fig. 4) originates from patch-to-patch variability, which has been reported before [14,30], even to a larger extent. We also performed a series of experiments in the outside-out configuration and identical global behavior was found as described here for the activated nAChR channel mutants in cell-attached patches (Fig. 1A). However, the excess standard deviation upon channel opening was less than 0.2 pA at 2.9 kHz bandwidth. In fact, the amplitudes of power spectra for open-states are not sufficiently larger than the background noise to allow subtraction and excess noise examination.

Therefore, analysis was conducted only on traces recorded in the cell-attached configuration. Since the resting cell membrane potential is added to the applied potential for each experiment, changes in the actual transmembrane voltage cannot be questioned. We presume that local changes in the pH value inside the cell would modulate the ionization state of the lysine 12' side chain, thus affecting the kinetics of fast current fluctuations.

#### 4.2. Voltage dependence

Previous studies have shown that the kinetics of nAChR channel gating varies with the membrane potential [62–66]. We found that the apparent equilibrium constant of open-channel gating  $O_1 \rightleftharpoons O_2$  decreases (Fig. 6A) and the frequency of full channel openings increases (Fig. 6B) with membrane hyperpolarization, while the relaxation time constant of the process is not affected (Fig. 4A, B). One possible model to quantify the voltage dependence is to regard the electric field strength  $E$  as a variable of state influencing the apparent equilibrium constant  $K$  according to Van't Hoff's relation [67]:

$$\frac{\partial \ln K}{\partial E} = \frac{\Delta M}{RT}, \quad (8)$$

where  $\Delta M$  is the molar reaction dipole moment, i.e. the change of the overall dipole moment of the system between the states  $O_1$  and  $O_2$ ,  $R$  is the gas constant and  $T$  the temperature. Integration delivers:

$$K = K_0 \exp(\alpha V); \alpha = -\frac{\Delta M}{dT}, \quad (9)$$

where  $K_0$  refers to the value of  $K$  at  $E=0$ ,  $V$  stands for the transmembrane voltage and  $d$  is the membrane thickness, assuming that the main voltage drop occurs over this region. A semilogarithmic representation of  $K$  as a function of  $V$  is shown in Fig. 6A. The parameters  $K_0$  and  $\Delta M$  are determined by fitting the experimental data with Eq. (9). For  $d=5$  nm and  $T=293$  K, the values are:  $K_0=20 \pm 2$  and  $\Delta M=26 \pm 6$  D, with no apparent difference for  $\gamma$ - and  $\epsilon$ -nAChRs within the accuracy of the measurements. Positive  $\Delta M$  indicates that the value of the axial component of the dipole decreases during transition from  $O_1$  to  $O_2$ . Similar values of  $\Delta M$  have been found in the gating of the rat myoball nAChR [65]. A more widely used model to examine the exponentially voltage dependence of equilibrium and rate constants is to define  $\alpha = z\delta F/RT$  in Eq. (9), where  $z$  is the mobile charge that moves during gating,  $\delta$  the fraction of the electric field crossed by  $z$  and  $F$  the Faraday's constant [53,66]. The fitted value of  $z\delta$  is  $0.11 \pm 0.01$  in the  $\gamma$ - and  $\epsilon$ -nAChRs, corresponding to the motion of one elementary charge across  $\sim 10\%$  of the membrane electrical field. Due to the large scattering of  $K$ , we do not exclude that a more complex model might describe the voltage influence, considering higher-order voltage dependent components such as molecular polarization and hyperpolarization coefficients [65,68,69]. Also, the exponential voltage dependence of  $K$  is only valid for the voltage range we investigated.

The ligand binding site is certainly located outside the electric field [70]. Although the ligands show specific slow- and fast-kinetic features, they exhibit identical voltage dependence. This result suggests that agonist-specific conformational changes are located outside the electric field, i.e. most probably outside the transmembrane region of the channel. No noticeable voltage dependence of the slow-kinetic gating was observed, suggesting also that the rate limiting steps of eventual gating charge-dipole movements in the protein responsible for the transition from the closed to open states are not located inside the membrane. On the contrary, the electric field influences the movement of charged moieties during channel opening from the intermediate state  $O_1 \rightarrow O_2$ . Therefore, the additional positive charge in the state  $O_1$  confers to the channel protein a larger voltage sensibility than in the state  $O_2$  in which the lysine 12' is deprotonated. This conclusion is valid for both direct and indirect interaction models. Note that in L-type  $Ca^{2+}$  channels, the proton exchange rate constants are voltage independent indicating that the proton binding site is not located inside the transmembrane electric field, i.e. outside the channel [56].

#### 4.3. Structure–function relationships

The conductance values of the first transition are significantly different for  $\gamma$ -nAChR and  $\epsilon$ -nAChR (12 and 25 pS, respectively), while values of the second transition are almost equal (28 and 32 pS, respectively) (Fig. 7). Therefore, structural determinants of the intermediate conductance of the mutated nAChR channel are likely to involve the TM2 domain in the  $\gamma$  or  $\epsilon$  subunit, the conductance of the second transition being preferentially controlled by other subunits. Key differences conferring higher conductance of the  $\epsilon$ -nAChR channel are the exchange of alanine (in  $\gamma$ ) for serine (in  $\epsilon$ ) at the 4' position and the substitution of lysine (in  $\gamma$ ) for glutamine (in  $\epsilon$ ) at the interface with the extracellular side (Fig. 8A) [28,54].

In the structure of closely related *Torpedo californica* nAChR (PDB code 2BG9) [36], the 12' residue of TM2 is not directed towards the channel lumen (Fig. 8B). In fact, it is rather oriented towards the adjacent  $\beta$  subunit as anticipated by Grosman and Auerbach [29] and is in close proximity to the positions 12' (leucine) in TM1 and 14' (phenylalanine) in TM2. However, it is important to point out that the structure in Fig. 8B does not represent the human receptor, but the *Torpedo californica* receptor and only a closed state thereof. Grosman and Auerbach suggested that insertion of hydrophilic residues at the 12' position in the mouse receptor could locally weaken the hydrophobic interactions contributing to the association of transmembrane helices, in the closed state and to a lower extent in the open state [29]. Consistently, the  $pK_a$  shift of the 12' lysine towards lower values ( $\Delta pK_a \sim -2$  relative to the value in bulk) reflects a surrounding environment of low dielectric constant in the open channel. Despite the flexibility of the lysine side chain, the mutation might introduce sterical hindrance between the  $\delta$  and  $\beta$  subunits during gating movements that could decrease the channel closing probability leading to long-lived open channel lifetimes.

Our data cannot distinguish whether TM2 segments undergo a rotation upon channel gating or a tilt relative to the channel axis. A detailed investigation on all residues lining the TM2 segment of the  $\delta$  subunit suggests that the side of the helix facing the channel lumen is the same in the closed and open states [22]. This hypothesis is supported by a recent normal mode analysis, which indicates that the global symmetrical twist of TM2 segments during channel gating does not result in the exposure of different residues towards the pore [71]. Our results imply that either  $\delta$  or  $\beta$  or both subunits undergo local conformational changes during gating transition. Indeed, the measured agonist and receptor type-specificities can be seen as support for a concerted mechanism of channel opening. This hypothesis is corroborated by data of ligand-induced fluorescence changes of a fluorophore attached to the 19' position of the  $\beta$  subunit [34] or SCAM experiments on the TM2 region of the  $\beta$  subunit [27].

## 5. Concluding remarks

It is known that internal protein motions occur in a broad range of time scales. Increasing the time resolution of current recordings is likely to unveil submicrosecond transition states of AChR gating [72,73]. Here, a single point mutation in the channel of the human nAChR leads to a sublevel of conductance, which can persist for several hundred milliseconds. Structural investigations of this mutant, regarded as a long-lived transition open channel, might provide information into structural dynamics of the TM2 segment and the gating process in general. Additionally, current fluctuations induced by proton exchange at a single residue side chain could be followed in time. Remarkably, the maturation state of the receptor and the nature of the bound agonist affect both processes in an apparently uncorrelated manner. How the mutation simultaneously influences the mechanism of channel gating and the translocation of cations is not clear. Novel insight might be delivered by combining single electrical channel recordings with single molecule fluorescence imaging using novel approaches to produce planar membranes and introducing stable fluorophores in the receptor [76,77].

## Acknowledgments

This work was supported by the European Commission via contract LSHG-CT-2004-504601 (E-MeP) and by the Swiss National Science Foundation (31-57023.99 and 31-00A0-102062/1).

## References

- [1] N.L. Absalom, T.M. Lewis, P.R. Schofield, Mechanisms of channel gating of the ligand-gated ion channel superfamily inferred from protein structure, *Exp. Physiol.* 89 (2004) 145–153.
- [2] E. Neher, B. Sakmann, Single-channel currents recorded from membrane of denervated frog muscle fibres, *Nature* 260 (1976) 799–802.
- [3] D.J. Nelson, F. Sachs, Single ionic channels observed in tissue-cultured muscle, *Nature* 282 (1979) 861–863.
- [4] B. Sakmann, J. Patlak, E. Neher, Single acetylcholine-activated channels show burst-kinetics in presence of desensitizing concentrations of agonist, *Nature* 286 (1980) 71–73.
- [5] D. Colquhoun, B. Sakmann, Fluctuations in the microsecond time range of the current through single acetylcholine receptor ion channels, *Nature* 294 (1981) 464–466.
- [6] S.J. Edelstein, O. Schaad, J.P. Changeux, Single binding versus single channel recordings: a new approach to study ionotropic receptors, *Biochemistry* 36 (1997) 13755–13760.
- [7] O.P. Hamill, B. Sakmann, Multiple conductance states of single acetylcholine receptor channels in embryonic muscle cells, *Nature* 294 (1981) 462–464.
- [8] A. Auerbach, F. Sachs, Flickering of a nicotinic ion channel to a subconductance state, *Biophys. J.* 42 (1983) 1–10.
- [9] A. Auerbach, F. Sachs, Single-channel currents from acetylcholine receptors in embryonic chick muscle. Kinetic and conductance properties of gaps within bursts, *Biophys. J.* 45 (1984) 187–198.
- [10] D.W. Tank, R.L. Haganir, P. Greengard, W.W. Webb, Patch-recorded single-channel currents of the purified and reconstituted Torpedo acetylcholine receptor, *Proc. Natl. Acad. Sci. U. S. A.* 80 (1983) 5129–5133.
- [11] O.P. Hamill, J. Bormann, B. Sakmann, Activation of multiple conductance state chloride channels in spinal neurones by glycine and GABA, *Nature* 305 (1983) 805–808.
- [12] S.G. Cull-Candy, M.M. Usowicz, Multiple-conductance channels activated by excitatory amino acids in cerebellar neurons, *Nature* 325 (1987) 525–528.
- [13] J.A. Van Hooft, H.P. Vijverberg, Phosphorylation controls conductance of 5-HT<sub>3</sub> receptor ligand-gated ion channels, *Recept. Channels* 3 (1995) 7–12.
- [14] F.J. Sigworth, Open-channel noise: I. Noise in acetylcholine receptor currents suggests conformational fluctuations, *Biophys. J.* 47 (1985) 709–720.
- [15] P. Luger, Structural fluctuations and current noise of ionic channels, *Biophys. J.* 48 (1985) 369–373.
- [16] Y. Kong, Y. Shen, T.E. Warth, J. Ma, Conformational pathways in the gating of *Escherichia coli* mechanosensitive channel, *Proc. Natl. Acad. Sci. U. S. A.* 99 (2002) 5999–6004.
- [17] B. Tanna, W. Welch, L. Ruest, J.L. Sutko, A.J. Williams, Voltage-sensitive equilibrium between two states within a ryanoid-modified conductance state of the ryanodine receptor channel, *Biophys. J.* 88 (2005) 2585–2596.
- [18] B. Prod'hom, D. Pietrobon, P. Hess, Direct measurement of proton transfer rates to a group controlling the dihydropyridine-sensitive Ca<sup>2+</sup> channel, *Nature* 329 (1987) 243–246.
- [19] S.M. Bezrukov, J. Kasianowicz, Current noise reveals protonation kinetics and number of ionizable sites in an open protein ion channel, *Phys. Rev. Lett.* 70 (1993) 2352–2355.
- [20] T.K. Rostovtseva, T.T. Liu, M. Colombini, V.A. Parsegian, S.M. Bezrukov, Positive cooperativity without domains or subunits in a monomeric membrane channel, *Proc. Natl. Acad. Sci. U. S. A.* 97 (2000) 7819–7822.
- [21] E.M. Nestorovich, T.K. Rostovtseva, S.M. Bezrukov, Residue ionization and ion transport through OmpF channels, *Biophys. J.* 85 (2003) 3718–3729.
- [22] G.D. Cymes, Y. Ni, C. Grosman, Probing ion-channel pores one proton at a time, *Nature* 438 (2005) 975–980.
- [23] F. Revah, D. Bertrand, J.L. Galzi, A. Devillers-Thiery, C. Mulle, N. Hussy, S. Bertrand, M. Ballivet, J.P. Changeux, Mutations in the channel domain alter desensitization of a neuronal nicotinic receptor, *Nature* 353 (1991) 846–849.
- [24] A. Villarroel, S. Herlitze, M. Koenen, B. Sakmann, Location of a threonine residue in the  $\alpha$ -subunit M2 transmembrane segment that determines the ion flow through the acetylcholine receptor channel, *Proc. R. Soc. Lond., B* 243 (1991) 69–74.
- [25] A. Villarroel, S. Herlitze, V. Witzemann, M. Koenen, B. Sakmann, Asymmetry of the rat acetylcholine receptor subunits in the narrow region of the pore, *Proc. R. Soc. Lond., B* 249 (1992) 317–324.

- [26] J. Chen, A. Auerbach, A distinct contribution of the  $\delta$  subunit to acetylcholine receptor channel activation revealed by mutations of the M2 segment, *Biophys. J.* 75 (1998) 218–225.
- [27] H. Zhang, A. Karlin, Contribution of the beta subunit M2 segment to the ion-conducting pathway of the acetylcholine receptor, *Biochemistry* 37 (1998) 7952–7964.
- [28] M.P. Sullivan, J.L. Owens, R.W. Kullberg, Role of M2 domain residues in conductance and gating of acetylcholine receptors in developing *Xenopus* muscle, *J. Physiol.* 515 (1999) 31–39.
- [29] C. Grosman, A. Auerbach, Asymmetric and independent contribution of the second transmembrane segment 12' residues to diliganded gating of acetylcholine receptor channels: a single-channel study with choline as the agonist, *J. Gen. Physiol.* 115 (2000) 637–651.
- [30] C. Grosman, A. Auerbach, Kinetic, mechanistic, and structural aspects of unliganded gating of acetylcholine receptor channels: a single-channel study of second transmembrane segment 12' mutants, *J. Gen. Physiol.* 115 (2000) 621–635.
- [31] C. Grosman, A. Auerbach, The dissociation of acetylcholine from open nicotinic receptor channels, *Proc. Natl. Acad. Sci. U. S. A.* 98 (2001) 14102–14107.
- [32] A. Mitra, G.D. Cymes, A. Auerbach, Dynamics of the acetylcholine receptor pore at the gating transition state, *Proc. Natl. Acad. Sci. U. S. A.* 102 (2005) 15069–15074.
- [33] G. Wilson, A. Karlin, Acetylcholine receptor channel structure in the resting, open, and desensitized states probed with the substituted-cysteine-accessibility method, *Proc. Natl. Acad. Sci. U. S. A.* 98 (2001) 1241–1248.
- [34] D.S. Dahan, M.I. Dibas, E.J. Petersson, V.C. Auyeung, B. Chanda, F. Bezanilla, D.A. Dougherty, H.A. Lester, A fluorophore attached to nicotinic acetylcholine receptor beta M2 detects productive binding of agonist to the alpha delta site, *Proc. Natl. Acad. Sci. U. S. A.* 101 (2004) 10195–10200.
- [35] A. Miyazawa, Y. Fujiyoshi, N. Unwin, Structure and gating mechanism of the acetylcholine receptor pore, *Nature* 423 (2003) 949–955.
- [36] N. Unwin, Refined structure of the nicotinic acetylcholine receptor at 4 Å resolution, *J. Mol. Biol.* 346 (2004) 967–989.
- [37] C.M. Gomez, R. Maselli, J.M. Williams, B.B. Bhattacharyya, R.L. Wollmann, J.W. Day, Genetic manipulation of AChR responses suggests multiple causes of weakness in slow-channel syndrome, *Ann. N. Y. Acad. Sci.* 841 (1998) 167–180.
- [38] C.M. Gomez, R.A. Maselli, B.P. Vohra, M. Navedo, J.R. Stiles, P. Charnet, K. Schott, L. Rojas, J. Keesey, A. Verity, R.W. Wollmann, J. Lasalde-Dominicci, Novel delta subunit mutation in slow-channel syndrome causes severe weakness by novel mechanisms, *Ann. Neurol.* 51 (2002) 102–112.
- [39] C.F. Newland, D. Beeson, A. Vincent, J. Newsom-Davis, Functional and non-functional isoforms of the human muscle acetylcholine receptor, *J. Physiol.* 489 (1995) 767–778.
- [40] F. Qin, A. Auerbach, F. Sachs, Estimating single-channel kinetic parameters from idealized patch-clamp data containing missed events, *Biophys. J.* 70 (1996) 264–280.
- [41] S. Elenes, A. Auerbach, Desensitization of diliganded mouse muscle nicotinic acetylcholine receptor channels, *J. Physiol.* 541 (2002) 367–383.
- [42] L.J. DeFelice, *Introduction to Membrane Noise*, Plenum Press, New York, 1981.
- [43] G. Feher, M. Weissman, Fluctuation spectroscopy: determination of chemical reaction kinetics from the frequency spectrum of fluctuations, *Proc. Natl. Acad. Sci. U. S. A.* 70 (1973) 870–875.
- [44] D. Colquhoun, A.G. Hawkes, K. Srodzinski, Joint distributions of apparent open and shut times of single-ion channels and maximum likelihood fitting of mechanisms, *Philos. Trans. R. Soc. Lond. A: Math. Phys. Eng. Sci.* 354 (1996) 2555–2590.
- [45] J. Grandl, C. Danelon, R. Hovius, H. Vogel, Functional asymmetry of transmembrane segments in nicotinic acetylcholine receptors, *Eur. Biophys. J.* (in press).
- [46] E. Yeramian, A. Trautmann, P. Claverie, Acetylcholine receptors are not functionally independent, *Biophys. J.* 50 (1986) 253–263.
- [47] A.M. Keleshian, R.O. Edeson, G.-J. Liu, B.W. Madsen, Evidence for cooperativity between nicotinic acetylcholine receptors in patch clamp records, *Biophys. J.* 78 (2000) 1–12.
- [48] R. Kullberg, J.L. Owens, P. Camacho, G. Mandel, P. Brehm, Multiple conductance classes of mouse nicotinic acetylcholine receptors expressed in *Xenopus* oocytes, *Proc. Natl. Acad. Sci. U. S. A.* 87 (1990) 2067–2071.
- [49] P. Camacho, Y. Liu, G. Mandel, P. Brehm, The epsilon subunit confers fast channel gating on multiple classes of acetylcholine receptors, *J. Neurosci.* 13 (1993) 605–613.
- [50] A.A. Carter, R.E. Oswald, Channel blocking properties of a series of nicotinic cholinergic agonists, *Biophys. J.* 65 (1993) 840–851.
- [51] S.M. Sine, J.H. Steinbach, Agonists block currents through acetylcholine receptor channels, *Biophys. J.* 46 (1984) 277–283.
- [52] A. Trautmann, Curare can open and block ionic channels associated with cholinergic receptors, *Nature* 298 (1982) 282–285.
- [53] G.J. Strecker, M.B. Jackson, Curare binding and the curare-induced subconductance state of the acetylcholine receptor channel, *Biophys. J.* 56 (1989) 795–806.
- [54] S. Herlitze, A. Villarroel, V. Witzemann, M. Koenen, B. Sakmann, Structural determinants of channel conductance in fetal and adult rat muscle acetylcholine receptors, *J. Physiol.* 492 (1996) 775–787.
- [55] D. Pietrobon, B. Prod'hom, P. Hess, Interactions of protons with single open L-type calcium channels: pH dependence of proton-induced current fluctuations with  $\text{Cs}^+$ ,  $\text{K}^+$ , and  $\text{Na}^+$  as permeant ions, *J. Gen. Physiol.* 94 (1989) 1–21.
- [56] B. Prod'hom, D. Pietrobon, P. Hess, Interactions of protons with single open L-type calcium channels: location of protonation site and dependence of proton-induced current fluctuations on concentration and species of permeant ions, *J. Gen. Physiol.* 94 (1989) 23–42.
- [57] S. Nekolla, C. Andersen, R. Benz, Noise analysis of ion current through the open and sugar-induced closed state of the LamB channel of *Escherichia coli* outer membrane: evaluation of the sugar binding kinetics to the channel interior, *Biophys. J.* 66 (1994) 1388–1397.
- [58] A.T. Ishida, J. Neyton, Quisqualate and L-glutamate inhibit retinal horizontal-cell responses to kainate, *Proc. Natl. Acad. Sci. U. S. A.* 82 (1985) 1837–1841.
- [59] S.G. Cull-Candy, M.M. Usowicz, Whole-cell current noise produced by excitatory and inhibitory amino acids in large cerebellar neurones of the rat, *J. Physiol.* 415 (1989) 533–553.
- [60] J.P. Dilger, R.S. Brett, Direct measurement of the concentration- and time-dependent open probability of the nicotinic receptor channel, *Biophys. J.* 57 (1990) 723–732.
- [61] H.P.C. Robinson, Y. Sahara, N. Kawai, Nonstationary fluctuation analysis and direct resolution of single channel currents at postsynaptic sites, *Biophys. J.* 59 (1991) 295–304.
- [62] S.M. Sine, T. Claudio, F.J. Sigworth, Activation of Torpedo acetylcholine receptors expressed in mouse fibroblasts. Single channel current kinetics reveal distinct agonist binding affinities, *J. Gen. Physiol.* 96 (1990) 395–437.
- [63] E. Neher, C.F. Stevens, Voltage-driven conformational changes in intrinsic membrane proteins, in: F.O. Schmitt, F.G. Worden (Eds.), *The Neurosciences: Fourth Study Program*, MIT Press, Cambridge, 1979, pp. 623–629.
- [64] M.B. Jackson, Kinetics of unliganded acetylcholine receptor channel gating, *Biophys. J.* 49 (1986) 663–672.
- [65] L.D. Chabala, Voltage dependence of acetylcholine receptor channel gating in rat Myoballs, *J. Gen. Physiol.* 100 (1992) 729–748.
- [66] A. Auerbach, W. Sigurdson, J. Chen, G. Akk, Voltage dependence of mouse acetylcholine receptor gating: different charge movements in di-, mono- and unliganded receptors, *J. Physiol.* 494 (1996) 155–170.
- [67] G. Schwarz, On the physicochemical basis of voltage-dependent molecular gating in biological membranes, *J. Membr. Biol.* 43 (1978) 127–148.
- [68] C.F. Stevens, Interactions between intrinsic membrane protein and electric field. An approach to studying nerve excitability, *Biophys. J.* 22 (1978) 295–306.
- [69] D. Marchais, A. Marty, Interaction of permeant ions with channels activated by acetylcholine in *Aplysia* neurones, *J. Physiol.* 297 (1979) 9–45.
- [70] K. Brejc, W.J. van Dijk, R.V. Klaassen, M. Schuurmans, J. van Der Oost, A.B. Smit, K. Sixma, Crystal structure of an ACh-binding protein reveals the ligand-binding domain of nicotinic receptors, *Nature* 411 (2001) 269–276.

- [71] A. Taly, M. Delarue, T. Grutter, M. Nilges, N. Le Novere, P.J. Corringer, J.P. Changeux, Normal mode analysis suggests a quaternary twist model for the nicotinic receptor gating mechanism, *Biophys. J.* 88 (2005) 3954–3965.
- [72] D.J. Maconochie, G.H. Fletcher, J.H. Steinbach, The conductance of the muscle nicotinic receptor channel changes rapidly upon gating, *Biophys. J.* 68 (1995) 483–490.
- [73] A. Auerbach, Life at the top: the transition state of AChR gating, *Sci. STKE* 188 (2003) re11.
- [74] S.M. Sine, X.-M. Shen, H.-L. Wang, K. Ohno, W.-Y. Lee, A. Tsujino, J. Brengmann, N. Bren, J. Vajsar, A.G. Engel, Naturally occurring mutations at the acetylcholine receptor binding site independently alter ACh binding and channel gating, *J. Gen. Physiol.* 120 (2002) 483–496.
- [75] C.J. Hatton, C. Shelley, M. Brydson, D. Beeson, D. Colquhoun, Properties of the human nicotinic receptor, and of the slow-channel myasthenic syndrome mutant  $\epsilon$ L221F, inferred from maximum likelihood fits, *J. Physiol.* 547 (2003) 729–760.
- [76] C. Danelon, J.-B. Perez, C. Santschi, J. Brugger, H. Vogel, Cell membranes suspended across nanoaperture arrays, *Langmuir* 22 (2006) 22–25.
- [77] E.G. Guignet, R. Hovius, H. Vogel, Reversible site-selective labeling of membrane proteins in live cells, *Nat. Biotechnol.* 22 (2004) 440–444.